$2p$ Photoionization of Atomic Ni: A Comparison with Ni Metal and NiO Photoionization

Kai Godehusen,* Tobias Richter, and Peter Zimmermann
Technische Universität Berlin, Hardenbergstrasse 36, D-10623 Berlin, Germany

Michael Martins†
Freie Universität Berlin, Arnimallee 14, D-14195 Berlin, Germany
(Received 28 November 2001; published 10 May 2002)

The photoabsorption spectrum of the $2p$-$3d$ resonances and the $2p$ photoelectron spectrum of atomic Ni were investigated both experimentally and theoretically. The analysis of the spectra takes into account that at the evaporation temperature of the metal at about 1800 K the fine structure states $3d^8\,4s^2\ ^3F$ and $3d^9\,4s\ ^3D$ of both configurations $3d^8\,4s^2$ and $3d^9\,4s$ are populated. The population of these two configurations offers the unique possibility for a comparison with the corresponding spectra in the condensed phase (Ni metal and NiO) where current configuration interaction calculations use the mixture of the configurations $(3d, 4s)^{10}$. By using our theoretical description of the $2p$ photoionization new insight into these condensed phase spectra is found.

DOI: 10.1103/PhysRevLett.88.217601 PACS numbers: 79.60.–i, 32.80.Fb, 32.80.Hd

The developments in synchrotron radiation facilities to provide intense, tunable, highly collimated, and polarized x-ray beams have stimulated the investigations of ferromagnetic materials by innershell photoemission experiments. Especially photoelectron spectroscopy due to its surface sensitivity is well suited to study the magnetic properties of multilayer systems or ultrathin films on ferromagnetic substrates. Modern techniques such as magnetic circular or linear dichroism in the angular distribution of photoelectrons (MCDAD or MLDAD) or spin-resolved photoelectron spectroscopy are used to obtain element- and site-specific information through the core-valence interactions [1–3].

In the case of the $2p$ photoionization of the $3d$ transition metals the key elements for the interpretation of these spectra are the $2p$ spin-orbit splitting of the core level and the core-valence interaction. The large $2p$ spin-orbit splitting of about 20 eV for the heavier $3d$ elements in general might favor the use of a single-particle approach [4]. Nevertheless, it is essential to keep in mind that there are very important atomic many-body effects in the p-shell photoelectron spectra of the transition metals [5,6]. Therefore it is crucial to have a proper understanding of the gas phase spectra for a critical comparison with the results of the condensed phase.

This paper reports on the $2p$ photoionization of atomic nickel. Ni in the gas phase exhibits a rather unique property that at the evaporation temperature of about 1800 K for the production of an atomic beam the lowest states $3d^8 4s^2\ ^3F$ and $3d^9 4s\ ^3D$ of *both configurations* $3d^8 4s^2$ *and* $3d^9 4s$ *are populated* (see Fig. 2). This offers the possibility for a comparison with corresponding spectra in the solid phase of Ni metal, Ni compounds, and molecular Ni complexes where the Ni ground state in many-body $3d$ configuration interaction (CI) calculations employing the Andersen impurity model is described as a mixture of $3d^{10}$, $3d^9$, and $3d^8$ valence configurations [7–10].

The experiments were carried out at the U49/2-PGM1 undulator beam line at the BESSY II electron storage ring in Berlin. By using electron bombardment the Ni metal was heated to about 1800 K forming an effusive atomic Ni beam. The linearly polarized synchrotron radiation intersected the atomic beam and either the resulting photoelectrons or the photoions were recorded.

For the detection of the photoelectrons a Scienta SES 200 hemispherical electron analyzer was used. For the detection of the photoions our experimental chamber also houses a time-of-flight (TOF) ion spectrometer. Therefore we were able to measure the ion yield at the $2p$-$3d$ resonances by scanning the photon energy and recording the intensity for the different ionic states of Ni.

The Ni $2p$ photoelectron spectrum is shown in Fig. 1 together with the results of our CI calculation.

The experimental spectrum consists of four main features which show additional structure. The spectrum is

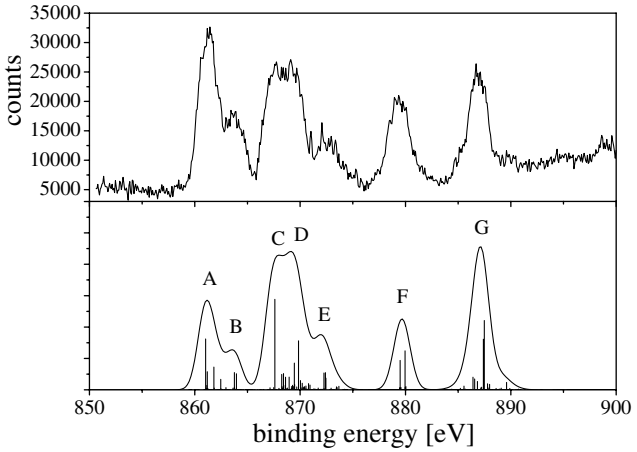

FIG. 1. Ni $2p$ photoelectron spectrum at $h\nu = 940$ eV and results of the HF calculation.

dominated by the spin-orbit interaction of the $2p$ hole (i.e., the splitting between the $2p_{3/2}$ and the $2p_{1/2}$ states) which is in the order of 20 eV. Additionally there are two different populations of the $3d$ shell (i.e., $3d^8$ and $3d^9$) which lead to a binding energy difference for these configurations of about 8 eV in the ionic state. That means that the virtual degeneracy of the ground states is canceled by the core hole. These two splittings ($2p_{3/2}$-$2p_{1/2}$ and $3d^8$-$3d^9$) are responsible for the four main features.

The additional structure seen in the experimental spectrum is due to the many-body interaction between the $2p$ and $3d$ shell and within the $3d$ shell. In the latter case the $3d$ shell does not remain in the $3d^8\,{}^3F$ state and the recoupling leads to an additional multiplet splitting up to some eV.

For a more detailed analysis of these interactions we did CI calculations of the atomic Ni $2p$ photoelectron spectrum.

For the theoretical Ni $2p$ spectrum the photoelectron spectrum for each of the six different ground states was calculated using the Cowan [11] code. The resulting bar spectra were convoluted with 1.7 eV wide Gaussians to match the experimental resolution. In Fig. 2 the $2p$ photoelectron spectra for the six different atomic ground states are depicted. Then the six spectra were scaled according to their relative population and added to yield the final theoretical spectrum shown in Fig. 1. One can easily see how the four main features in the experimental spectrum (Fig. 1) are connected to the different populations of the $3d$ shell.

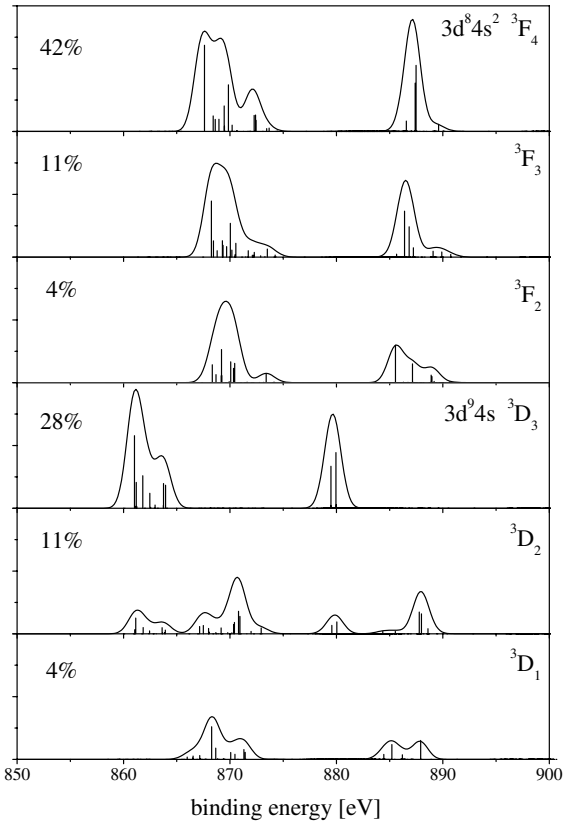

FIG. 2. Calculated Ni $2p$ photoelectron spectra for the six populated ground states. The percentage shown is the relative contribution of the respective spectrum to the final Ni $2p$ spectrum (lower panel of Fig. 1).

Our configuration interaction (CI) calculations using Hartree-Fock (HF) wave functions as zero-order approximation contain the configuration interaction with states where one or two $4s$ electrons are excited to $3d$ or $4p$, in the atomic ground state as well as in the ionic ($2p$ hole) state. It was necessary to include these CI in order to reproduce the experimental spectrum by our calculations. In this way, in spite of the high complexity of the calculations, we have reached an excellent agreement. One should mention that the binding energies are slightly overestimated by the calculation. We therefore shifted the spectra for the $3d^8 4s^2$ ground state by 0.51 eV and the spectra for the $3d^9 4s$ ground state by 1.7 eV to the lower binding energy side. The relative shift between the different ground state configurations is due to correlation contributions not completely taken into account by our calculation and which depend strongly upon the configuration of the $3d$ and $4s$ shell. It is well known that the $3d$ transition metal atoms pose extreme difficulties for the exact *ab initio* calculation of ground state energies [12–14]. This shift had only to be corrected in our calculated atomic spectra, in the comparison of the atomic and solid state experimental spectra, later discussed, such a shift does not exist.

Table I displays the assignment of the calculated electron lines that dominate the four main features and some of the additional structure. One can easily assign these four main features ($A + B$, $C + D + E$, F, and G) to the $2p_{1/2}$ and $2p_{3/2}$ holes of the $3d^8$ and $3d^9$ states, as shown in the lower graph of Fig. 3. Ionic states with a $3d^{10}$ configuration have also been included in our calculation, but have not been significantly populated.

From Fig. 2, it can be seen that the configuration $3d^8 4s^2$ is stable during the $2p$ ionization (top three panels of Fig. 2), all the lines have a configuration of $2p^5 3d^8 4s^2$. But in the case of the configurations $3d^9 4s\,{}^3D_2$ and $3d^9 4s\,{}^3D_1$ Fig. 2 shows that these configurations partially or completely break up during photoionization, which can easily be seen from the energy position of the resulting $2p^{-1}$ lines. This is no ground state effect due to the high purities of the states (see [15]).

Now that we are able to describe the $2p$ photoemission from atomic Ni, we can compare these results to the photoemission spectra of NiO and Ni metal. Figure 3 presents the Ni $2p$ spectrum from Fig. 1 together with the $2p$ spectra of NiO from [16] and Ni metal from [17].

We will focus on the striking similarity between the spectra of atomic Ni and NiO. The spectrum from Parmigiani and Sangaletti [16] was taken from a NiO single crystal at grazing angle. It exhibits the same four main features and the same additional structure as the atomic spectrum. This is strong evidence for a localized character of the $3d$ orbitals in NiO. Parmigiani and Sangaletti

TABLE I. Table of the strongest lines in the calculated Ni $2p$ spectrum. The intensity is relative to the line in feature C and the initial state denotes from which ground state these lines are populated.

Feature	Binding energy [eV]	Ionic state	Relative intensity	Initial state
A	861.03	$2p^5 3d^9 4s\ ^4F_{9/2}$	0.56	$3d^9 4s\ ^3D_3$
	861.19	$2p^5 3d^9 4s\ ^2D_{5/2}$	0.20	$3d^9 4s\ ^3D_3$
	861.81	$2p^5 3d^9 4s\ ^4D_{7/2}$	0.25	$3d^9 4s\ ^3D_3$
B	863.76	$2p^5 3d^9 4s\ ^2F_{7/2}$	0.19	$3d^9 4s\ ^3D_3$
	863.95	$2p^5 3d^9 4s\ ^2P_{3/2}$	0.18	$3d^9 4s\ ^3D_3$
C	867.60	$2p^5 3d^8 4s^2\ ^4G_{11/2}$	1.00	$3d^8 4s^2\ ^3F_4$
D	869.45	$2p^5 3d^8 4s^2\ ^4F_{7/2}$	0.29	$3d^8 4s^2\ ^3F_4$
	869.85	$2p^5 3d^8 4s^2\ ^4F_{9/2}$	0.23	$3d^8 4s^2\ ^3F_4$
E	872.27	$2p^5 3d^8 4s^2\ ^2F_{7/2}$	0.19	$3d^8 4s^2\ ^3F_4$
	872.40	$2p^5 3d^8 4s^2\ ^2D_{5/2}$	0.19	$3d^8 4s^2\ ^3F_4$
	872.44	$2p^5 3d^8 4s^2\ ^2G_{9/2}$	0.13	$3d^8 4s^2\ ^3F_4$
F	879.49	$2p^5 3d^9 4s\ ^4P_{5/2}$	0.33	$3d^9 4s\ ^3D_3$
	879.96	$2p^5 3d^9 4s\ ^4F_{7/2}$	0.43	$3d^9 4s\ ^3D_3$
G	887.40	$2p^5 3d^8 4s^2\ ^4D_{7/2}$	0.56	$3d^8 4s^2\ ^3F_4$
	887.49	$2p^5 3d^8 4s^2\ ^2G_{9/2}$	0.77	$3d^8 4s^2\ ^3F_4$

could partially describe their spectrum by applying local and nonlocal screening models. For example, the splitting of the main line of NiO at about 854 eV binding energy (upper scale) was explained as a special effect [16,18] due to nonlocal screening [16]. In the atomic case this splitting corresponds to the splitting between feature A and B and is explained by the different couplings of the $3d^9$ shell with the $2p$ hole. As this could also be valid for the splitting seen in NiO, we do not see any evidence that this explanation cannot also be applied to the condensed phase.

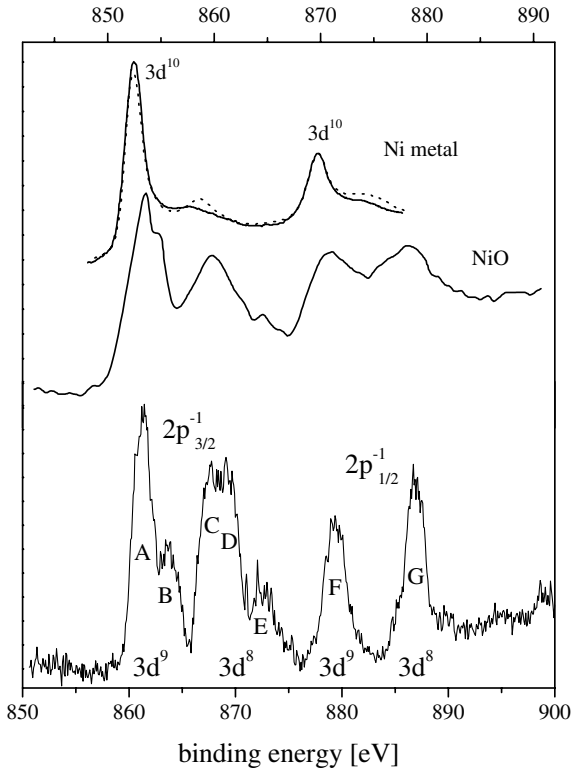

FIG. 3. Ni $2p$ photoelectron spectrum at $h\nu = 940$ eV, compared with NiO [16] and Ni metal (after [17] taken from [19], dotted line: majority states, solid line: minority states). The energy scale on top is valid for Ni and NiO, whereas the lower scale belongs to atomic Ni.

In Fig. 3 also a photoelectron spectrum of Ni metal is depicted (after [17] taken from [19]), it is a spin-resolved spectrum showing the contributions of the majority and minority states. The two main features seen are attributed to $2p^5 3d^{10}$ ionic states and the two more shallow features to $3d^9$ [17]. Obviously the spectrum of Ni metal is very distinct from that of NiO and atomic Ni. Therefore the comparison with NiO and atomic Ni spectra leads to the conclusion that the $3d$ orbitals in Ni metal show strong nonlocal character.

Using the same CI calculation approach as before, we were also able to fully reproduce the $2p$ absorption spectrum of atomic Ni with our theoretical description including the calculation of the linewidth by calculation of the subsequent Auger decay. Figure 4 presents the ion yield spectrum of atomic Ni together with the results of the calculation and a comparison to absorption spectra of Ni metal and NiO films. Neglecting fluorescence decays into neutral Ni, this ion yield is directly proportional to the absorption spectrum. It can be easily seen that despite the fact that atomic Ni has some more resonance lines in the $2p_{3/2}$ peak the spectra are remarkably similar. In the case of the absorption spectrum the influences of the different populations of the $3d$ shell are small compared to the photoelectron spectra. The assignment of the four main lines in the $2p_{3/2}$ peak (at 852 eV) with ascending photon energy

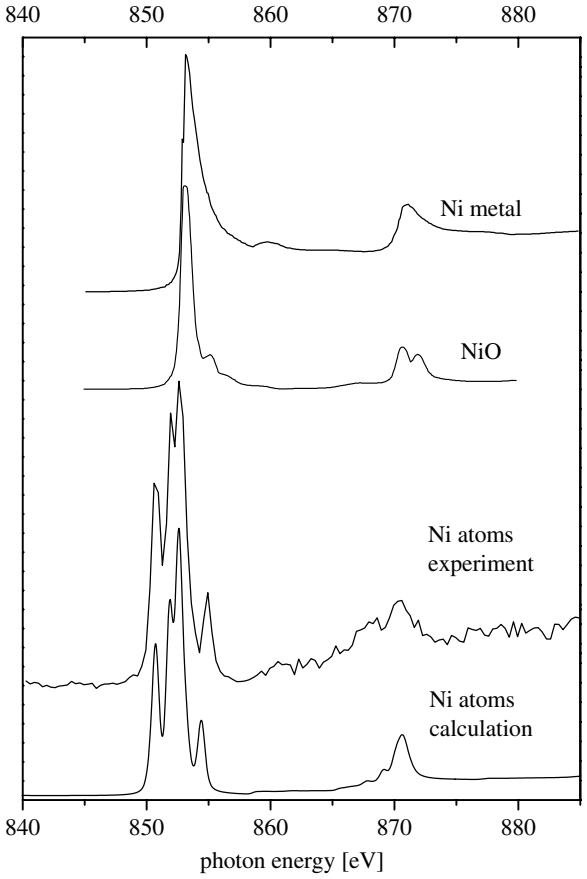

FIG. 4. Ni $2p$ absorption spectrum, compared with Ni film on Co/Cu(001) [20] (only parallel spectrum shown) and 20 ML NiO on MgO [18].

is $3d^{10}4s\,^3P_2$, $3d^9 4s^2\,^3F_4$, $^3D_3$, and $^1F_3$. In the case of atomic Ni the $2p_{1/2}$ absorption line consists of the superposition of several atomic states and no simple assignment can be given.

In conclusion, we can say that the investigation of the $2p$ photoionization of atomic Ni, presented in this paper for the very first time, has lead to a better understanding not only of the photoionization process of Ni atoms but also of Ni metal and compounds. We were able to fully comprehend the atomic spectra by CI calculations and on this basis new insight on the character of the $3d$ shell in Ni metal and NiO could be provided.

The authors would like to thank the BESSY staff for their support during the beam times and the Deutsche Forschungsgemeinschaft (DFG) for their funding.

*Present address: BESSY GmbH, Albert-Einstein-Strasse 15, D-12489 Berlin, Germany.
†Present address: Universität Hamburg, Luruper Chaussee 149, D-22761 Hamburg, Germany.

[1] L. Baumgarten, C. M. Schneider, M. Petersen, F. Schäfers, and J. Kirschner, Phys. Rev. Lett. **65**, 492 (1990).
[2] C. Roth, F. U. Hillebrecht, H. B. Rose, and E. Kisker, Phys. Rev. Lett. **70**, 3479 (1993).
[3] F. U. Hillebrecht, R. Jungblut, and E. Kisker, Phys. Rev. Lett. **65**, 2450 (1990).
[4] J. G. Menchero, Phys. Rev. B **57**, 993 (1998).
[5] G. van der Laan, S. S. Dhesi, and E. Dudzik, Phys. Rev. B **61**, 12 277 (2000).
[6] P. S. Bagus, R. Broer, W. A. de Jong, W. C. Nieuwport, F. Parmigiani, and L. Sangaletti, Phys. Rev. Lett. **84**, 2259 (2000).
[7] B. T. Thole and G. van der Laan, Phys. Rev. Lett. **67**, 3306 (1991).
[8] G. van der Laan, M. A. Hoyland, M. Surman, C. F. J. Flipse, and B. T. Thole, Phys. Rev. Lett. **69**, 3827 (1992).
[9] G. van der Laan, M. Surman, M. A. Hoyland, C. F. J. Flipse, B. T. Thole, Y. Seino, H. Ogasawara, and A. Kotani, Phys. Rev. B **46**, 9336 (1992).
[10] A. Tanaka, T. Jo, and G. A. Sawatzky, J. Phys. Soc. Jpn. **61**, 2636 (1992).
[11] R. Cowan, *The Theory of Atomic Structure and Spectra* (University of California Press, Berkeley, 1981).
[12] C. Froese Fischer, J. E. Hansen, and M. Barwell, J. Phys. B **9**, 1841 (1976).
[13] C. Froese Fischer and R. Glass, Phys. Scr. **21**, 525 (1980).
[14] O. V. Gritsenko, N. A. Cordero, A. Rubio, L. C. Balbas, and J. A. Alonso, Phys. Rev. A **48**, 4197 (1993).
[15] C. E. Moore, *Atomic Energy Levels* (National Standard Reference Data System, NSRDS-NBS 35, 1971).
[16] F. Parmigiani and L. Sangaletti, J. Electron. Spectrosc. Relat. Phenom. **98-99**, 287 (1999).
[17] J. G. Menchero, Phys. Rev. B **76**, 3208 (1996).
[18] D. Alders, F. C. Voogt, T. Hibma, and G. A. Sawatzky, Phys. Rev. B **54**, 7716 (1996).
[19] A. K. See and L. E. Klebanoff, Phys. Rev. B **51**, 11 002 (1995).
[20] S. S. Dhesi, H. A. Dürr, G. van der Laan, E. Dudzik, and N. B. Brookes, Phys. Rev. B **60**, 12 852 (1999).